Proceedings of OMAE2005
24th International Conference on Offshore Mechanics and Arctic Engineering (OMAE 2005)
June 12-17, 2005, Halkidiki, Greece

OMAE2005-67252

BENCHMARKING OF TRUSS SPAR VORTEX INDUCED MOTIONS DERIVED FROM CFD WITH EXPERIMENTS

John Halkyard, Senu Sirnivas
Technip Offshore, Inc. Houston Texas
Samuel Holmes, Applied Research Associates, Mountain View, California
Yiannis Constantinides, Owen Oakley
ChevronTexaco, Houston, Texas & San Ramon, California
Krish Thiagarajan, University of Western Australia, Perth

ABSTRACT

Floating spar platforms are widely used in the Gulf of Mexico for oil production. The spar is a bluff, vertical cylinder which is subject to Vortex Induced Motions (VIM) when current velocities exceed a few knots. All spars to date have been constructed with helical strakes to mitigate VIM in order to reduce the loads on the risers and moorings. Model tests have indicated that the effectiveness of these strakes is influenced greatly by details of their design, by appurtenances placed on the outside of the hull and by current direction. At this time there is limited full scale data to validate the model test results and little understanding of the mechanisms at work in strake performance. The authors have been investigating the use of CFD as a means for predicting full scale VIM performance and for facilitating the design of spars for reduced VIM. This paper reports on the results of a study to benchmark the CFD results for a truss spar with a set of model experiments carried out in a towing tank. The focus is on the effect of current direction, reduced velocity and strake pitch on the VIM response. The tests were carried out on a 1:40 scale model of an actual truss spar design, and all computations were carried out at model scale. Future study will consider the effect of external appurtenances on the hull and scale-up to full scale Reynolds' numbers on the results.

INTRODUCTION

Floating spar platforms are widely used in the Gulf of Mexico for oil production. Three types of spars are in use: classic, truss and cell. These configurations are illustrated in fig. 1.

Three classic spars currently are in use. They are circular cylinders, approximately 700 ft long with diameters of 72 and 122 ft. The truss spars are similar in overall dimensions, but the circular cylinder is truncated and the lower part of the hull consists of an open truss structure. The cell spar is the newest generation of spar platform. It consists of a cluster of smaller cylinders. In all cases the spars float vertically, and are held in place by mooring lines which are attached close to mid-draft of the hull. More details on these spar design may be found in [1,2,3].

Spar mooring systems permit motions in six degrees of freedom: surge, sway, heave, roll, yaw and pitch, however, surge and sway are the dominant motions in current-induced VIM. For the purposes of this paper surge is assumed to correspond to be in-line with the current. VIM lock-in occurs when the reduced velocity, U_{rn}, is in a critical range called "lock-in" [4].

$$U_{rn} = \frac{uT_n}{D} \qquad (1)$$

In lock-in the sway motion (transverse to the current) of a cylinder oscillates with a period close to Tn, and with an amplitude that can approach the spar diameter. Mean drag increases proportional to the amplitude of this motion. Figure 2 shows a typical plot of the amplitude to diameter ratio, A/D, for a classic and truss spar, with and without helical strakes as measured in scale model tests.

Figure 2 compares the motions of spars modeled as plane circular cylinders both with and without helical strakes. In reality, actual spars are not plane circular cylinders, but rather their geometries are much more complex. For example, their hulls are covered with anodes, various pipes are attached to the outside of the hull, holes are placed in the strakes to allow mooring chain to pass along the hull, etc. These appurtenances and geometric variations may result in a significant deterioration in the performance of the strakes which has been well documented in the literature [5-8]. This could be a significant issue in the design of the spar and the mooring systems. [For example, if the mooring system design is controlled by the spar's response in currents, the amplitude of VIM and the associated drag enhancement could be the most important determinant in the design of the mooring system.] Figure 3 shows a typical mooring system (left) and displacement trajectories at various current speeds from a scale model experiment. The lateral motions can cause peak tensions which may control the mooring line breaking strength

requirements in design, and repeated cyclic loadings could introduce fatigue critical loadings.

There is presently no generally accepted analytical method for predicting the VIM behavior of spar platforms. Furthermore, most spar designs have a unique configuration of strakes and appurtenances. Standard design practice has been to use model tests to obtain the necessary design data. These tests are costly and require a long lead time. The purpose of the research described in this paper is to determine whether CFD can be used as a proxy for model tests, if not for the final design, at least to perform optimization studies at an early stage of the design.

In what follows we first describe a set of model tests on a typical truss spar that was performed using a towing facility. Tests on the same model were subsequently performed in an ocean basin with flowing current. Results from the experiments form the basis for this validation exercise. The tests were performed at a 1:40 scale using Froude scaling, and all CFD runs were done in model scale. Scale-up runs will be performed after model tests have been benchmarked and it should be noted that the results presented here are preliminary as this work is ongoing.

NOMENCLATURE

L = Characteristic length of truss
M = Mass of spar
M* = Mass ratio
u = Current velocity magnitude
$\vec{u}$ = Current velocity vector
$\vec{U}$ = Relative velocity vector
U_{rn} = Reduced velocity based on calm water period
T_n = Natural period in calm water without current
D = Diameter
ρ = density of water
$\dot{\vec{x}}$ = Spar velocity vector
$\forall$ = volumetric displacement of spar

EXPERIMENTS

The experimental model consisted of a hard tank cylinder with a diameter, D, equal to 0.741 m, a 1.4 m draft, and a truss section which extended the total draft to 3.8 m. Towing tests were carried out by Force Technology (formerly the Danish Maritime Institute). Figure 4 shows photos of the model used for these benchmarks. The model was free floating and connected to a towing carriage by four linear springs representing the stiffness of mooring lines. Figure 5 shows a side view of this arrangement. Tests were conducted for a Reynold's number range of 40,000 – 150,000, and at reduced velocities between 3 and 11. A companion paper [9] presents further details of these tests.

Two strake configurations were used for CFD comparisons. The main difference was in the pitch of the strakes. Configuration A has a pitch of 4.5D. The start and stop points of the strakes at the bottom of the hard tank corresponded to the same azimuth, i.e. each strake covered exactly 1/3 of the circumference. Configuration B had a pitch of 3.5D. These strakes overlapped about 30%, i.e. each strake covered about 43% of the circumference. Model tests have shown that Configuration B resulted in better performance. One objective of this work was to determine if CFD would predict the same affect.

The spar is free floating, i.e. the mass of the spar nearly equals the displacement of water. The vertical component of the mooring lines is negligible. Hence the mass ratio, M^*, is equal to one.

$$M^* = \frac{M}{\rho \forall} \tag{2}$$

Figure 6 shows the measured responses of these tests for the two configurations. The three peaks in the response, particularly for Configuration A, can be attributed to direction where the helical strakes lose their effectiveness because streamlines are not separating at the strakes, but rather from the cylinders surface. These "hot spots" are approximately 120 degrees apart. This observation was verified by CFD and discussed later. This behavior is typical of strakes of this type. Configuration B doesn't show this periodicity, although two clear hot spots remain. They are not exactly 120 degrees apart, however.

CFD CALCULATIONS

All of the solutions shown here were produced using AcuSolve™. AcuSolve™ is a finite element CFD solver. It is based on the Galerkin/Least Squares formulation and supports a variety of element types. AcuSolve™ uses a fully coupled pressure/velocity iterative solver plus a generalized alpha method as a semi-discrete time stepping algorithm [10]. AcuSolve™ is second order accurate in space and time.

Turbulence was modeled using Spalart's version of detached eddy simulation (DES). This DES model is based on the one-equation turbulence model of Spalart-Allmaras [11] Near the wall the model acts like the S-A Reynolds averaged Navier Stokes (RANS) model and far from the wall it behaves similarly to large eddy simulation (LES) models. As implemented in AcuSolve™, DES transitions smoothly from RANS to LES configurations. The constants required are not listed here but are those suggested by Spalart. It should be noted that a feature of this turbulence model is that at points away from the wall, unresolved (subgrid scale) turbulence is assumed to be isotropic and the eddy viscosity is a function of element size. A danger at the high Re of the problems solved here is that this last assumption is not met. We used wall functions to describe the flow at the wall in all CFD simulations. This was done to economize on mesh size, but also because both model tests and the full scale spar have rough surfaces.

Figure 8 shows a typical mesh used in the simulations. As shown, the fluid domain is a parallelepiped with inlet and outlet planes. The mesh is designed with small grid spacing in the wake and relatively coarse grid spacing elsewhere in to provide an economical grid. Note that the lower truss portion of the

model is not modeled explicitly. Rather, we created user defined function for the motion of the spar which estimated the effects of the truss using Morison's equations. This function will be described shortly. The economies of the omitting the truss and carefully defining the mesh allowed the use of relatively small meshes. Each grid contained approximately 520,000 nodes and 520,000 hexahedral elements. Typical run times for 2000 time steps, or about 30 vortex shedding cycles (equivalent to the length of experiments), on an 8 CPU Linux P4 cluster using a gigabit switch are on the order of 24 hours.

The meshes used here were designed to place the first nodes away from the wall just above the surface roughness on the model. In this application, k_s is quite large relative to diameter so the use of wall functions reduces problem size significantly. On the other hand, this type of mesh also tends to produce average calculated values of y^+ on the order of 20 with maximum values sometimes approaching 100, or larger than usually recommended for smooth cylinders. At this time the alternative is to model the surface roughness explicitly which would be cost prohibitive.

The hybrid fluid structure interaction model used to solve for the motion of the spar and avoid explicit modeling of the truss was based on Morison's equation. The user function modeled the mooring system used in the tow tank explicitly. Morison's equation was used to compute the hydrodynamic force on the truss.

$$\vec{F} = \frac{1}{2}\rho C_d L^2 \vec{U}\left|\vec{U}\right| + \rho C_a L^3 \frac{\partial \vec{U}}{\partial t} \quad (3)$$

$$\vec{U} = \vec{u} - \dot{\vec{x}} \quad (4)$$

Here the force vector is calculated by assuming that the force on the truss arises from drag and added mass (acceleration) contributions. The drag contribution (the first term on the right hand side) is determined by a drag coefficient C_d , a characteristic length scale L, and the spar velocity relative to the free stream velocity U. Note that the drag coefficient must include the projected area when multiplied by the characteristic length. The added mass term is formed in a similar manner. As implemented here, we did not account for the changes in the added mass and drag coefficients with the direction of mass or acceleration relative to the free stream flow although this could be done.

In the simulations, the motion of the spar is calculated within each time step by first determining the integral of the surface tractions of on the hard tank from the CFD solution. This is provided by the AcuSolve flow solution. The forces due to the mooring system are calculated from the current spar position and forces on the truss are calculated from the current velocity and kinematics of the spar with respect to the free stream current. The new position of the spar for the next time step is found by a simple integration using the trapezoidal rule. In effect, the new position of the spar is calculated using the force values at the middle of the step.

The motion of the spar within the mesh is accommodated using a specified mesh motion in which the position of each node is specified based on the spar position. This approach avoids the solution of nodal locations using an arbitrary elastic solid to represent the mesh (Arbitrary Langrangian Eulerian or ALE method) and hence solve for the new nodal locations. However, the fluid flow is calculated based on the new nodal locations as in the ALE method.

The coefficients for truss and soft tank added mass and drag were derived from formulations for fixed jacket structures in API RP2A and from previous model test programs. Sensitivity of the results to truss coefficients was examined. Also, the sensitivity to a pseudo-shear current was examined by setting U equal to zero in this equation. Future work will include explicit modeling of the truss as well.

RESULTS

Figures 10 and 11 show time series comparisons for two cases for configuration A with the large responses (150 deg) and small responses (330 deg) respectively. Angles are defined in fig. 7. The upper plot is for the transverse motion. The bottom plot shows the trajectory. In the former case CFD predicts a higher response, and the shape of the trajectory shows a convex "banana" shape compared to the slightly concave shape for the experiment. The shape of the response is dictated by the phasing between in-line and transverse forces. For the higher responses, the experiment shows higher modulation than CFD. This might be caused by the effect of chains on the flow around the cylinder; however we have not run CFD which includes the chains. The fact that the mean offsets are different between the CFD and experiments is not relevant, insofar as the experiments were conducted with an in-line force balance to keep the model centered in the test rig.

Directional results for Configurations A and B are shown in fig. 12-13, respectively. These plots show the standard deviation of the responses at the maximum response. CFD results are shown replicated at 120 degree intervals as the model has symmetry about these directions. Hot-spot directions are clearly identified with the CFD, however CFD predicts higher peak at the hot spots than the experiments. Figure 14 shows the relationship of A/D vs. U_{rn} for the most responsive direction for configuration A. CFD predicts earlier lock-in and higher amplitudes.

SENSITIVITY CASES

Several sensitivity cases were run to determine the effect of changing the model. Table 1 shows the results for the transverse A/D from these cases. All of these runs were for Configuration A at 150 deg and a U_{rn} of 7, one of the highest response cases. The results for truss drag sensitivity are also plotted on fig. 12. From the figure, it appears the high drag case (2 times the nominal) comes very close to the experimental result at 157.5 degrees, even though it is double the experiment at 150 degrees. Further runs with a more detailed model are required to see if this is an issue with angular resolution.

A mesh sensitivity comparison with 1.6M nodes versus 520,000 nodes did not show any large affect, although the higher mesh sensitivity has only been run for about three cycles as of this writing. Doubling the drag coefficient on the truss showed a 33% reduction in the RMS amplitude of the response. Eliminating the truss drag increased the RMS response by 30%. A shear current was simulated by setting u equal to zero in equation 4. In effect this reduced the damping of the truss due to the vector sum of the inflow velocity and the kinematics, although damping due to the truss moving in still water remained. The response in this case increased by about 20%.

Although the sensitivities appear reasonable, all of the cases exceed the observed results from the tests.

DISCUSSION

These comparisons show good agreement for the directional sensitivity of the results and for the effect of pitch angle. Flow visualization shows that the reason for better strake performance from certain directions is the migration of the flow separation from the cylinder surface to the strake edges in certain directions. Figure 15 shows an iso-pressure surface generated for a run with the largest response. The sequence covers a single cycle of motions. The iso-pressure surface may be considered a proxy for a vortex core or separated eddy. The sequence shows the flow separating first from the edge of the strake, then from the surface of the cylinder. Where strakes are effective the separation appears to occur at the edge of the strakes as seen in fig. 16. Coherent vortices do not appear downstream. The flow in fig. 16 appears similar to that shown by Bearman [12] for flow visualization for a fixed straked cylinder. When the strakes are not as effective, the motion of the cylinder results in a coherent vortex in the wake, also consistent with Bearman's observations. The "hot spots" are generally related to a particular azimuth from the strake starts and are 120 degrees separated. This is clear for Configurations A and B in fig. 6. Presumably, the hot spots are related to a particular azimuth where a preponderance of streamlines are allowed to escape the edge of the strakes before they encounter the cylinder, and are allowed to form boundary layers and introduce vorticity from the cylinder's edge.

CONCLUSIONS AND RECOMMENDATIONS

The performance of helical strakes in water, especially at low mass ratios, is known to be less effective than similar geometries in air [12]. The problem for spar designers is to quantify this effectiveness in the design process early enough to be able to select the appropriate configuration of the hull and mooring. This effort to validate CFD against model tests has proven the potential for this, but more work remains. CFD does indeed identify "hot spots" and differences in the effectiveness of different strake configurations. The magnitude of responses in the hot spots seems to be overpredicted by CFD, at least when compared with model scale results in this example. It remains to determine the reasons for this and whether better modeling techniques could improve this agreement. Since it appears that the occurrence of hot spots is related to separation of the flow from the body of the spar as opposed to the strake edges, CFD modeling issues involve boundary layer phenomena including wall effects, surface roughness and turbulence. These are among the most difficult problems facing the CFD community. We also have not tackled the subtle effects of adding roughness or appendages to the spar hull. These have been shown critical in predicting the VIM response [8, 13, 14]. We will shortly be expanding our model to include the chains and an explicit representation of the truss structure. Extrapolation of these results to full scale requires a leap of faith, in that full scale or even very high Reynold's number data is sorely missing.

Work is ongoing to expand the experimental database upon which to validate CFD. Our goal is to bring this technology to practical application for these problems within the next year. Future projects may be able to realize some measure of predictive capability for VIM before having to wage a major test program.

REFERENCES

[1] Vardeman, R.D., Richardson, S., and McCandless, C.R., 1997, "Neptune Project: Overview and Project Management," Proceedings Offshore Technology Conference, Houston, Texas, Paper Number OTC 8381.

[2] Bangs, A. S., Miettinen, J. A., Mikkola, T. P. J., Silvola, I., and Beattie, S. M., 2002, "Design of the Truss Spars for the Nansen/Boomvang Field Development," Proceedings Offshore Technology Conference, Houston, Texas, Paper Number OTC 14090.

[3] Finn, L. and Maher, J., 2003, "The Cell Spar for Marginal Field Developments," Proceedings Deep Offshore Technology Conference, Marseille, France.

[4] Blevins R.D., 1990, Flow-Induced Vibration, Van Nostrand Reinhold, New York.

[5]Mercier, R.S. and Ward, E. G., 2004, "Spar Vortex-Induced Motions Workshop – Proceedings", Offshore Technology Research Center, Texas A&M University, in preparation.

[6] Magee, A., Sablok, A., and Gebara, J., 2003, "Mooring Design for Directional Spar Hull VIV," Proceedings Offshore Technology Conference, Paper Number OTC 15243.

[7] van Dijk, R., Magee, A., Perryman, S., and Gebara, J., 2003, "Model Test Experience on Vortex Induced Vibrations of Truss Spars", Proceedings Offshore Technology Conference, Paper Number OTC 15242.

[8] Irani, M. and Finn, L., 2004, "Model Testing for Vortex Induced Motions of Spar Platforms", Proceedings 23rd International Conference on Offshore Mechanics and Arctic Engineering, OMAE'04-51315, Vancouver, B.C., Canada

[9] Irani, M. and Finn, L., 2005, "Improved Strake Design for Vortex Induced Motions of Spar Platforms", Proceedings 24th International Conference on Offshore Mechanics and Arctic Engineering, OMAE'05-67384, Halkidiki, Greece

[10] Jansen, K. E., Whiting, C. and Hulbert, G. M., 2000, "A generalized-alpha method for integrating the filtered Navier-Stokes equations with a stabilized finite element method", *Computer Methods in Applied Mechanics and Engineering.*

[11] Spalart, P. R. and Allmaras, S. R., 1992, "A one-equation model for aerodynamic flows," AIAA 92-0439

[12] Bearman, P. and Branković, M., 2002, "Passive Control of Vortex Induced Vibration", Proceedings Conference

on Bluff Body Wakes and Vortex-Induced Vibrations (BBVIV3), Port Douglas, Australia

[13] Yung, T.W., Sandstrom, R.E., Slocum, S.T., and Ding, J.Z., 2003, "Advances in Prediction of VIV on Spar Hulls," Proceedings Deep Offshore Technology Conference, Marseille, France.

[14] Oakley, O., Constantinides, Y., Navarro, C. and Holmes, S., 2005, "Modeling Vortex induced Motions of spars In uniform and stratified flows", Proceedings 24th International Conference on Offshore Mechanics and Arctic Engineering, OMAE'05-67238, Halkidiki, Greece.

	Std	(Max-Min)/2
Nominal	0.24	0.41
Mesh Sensitivity: 1.6MM Nodes	0.21	0.38
Double Truss Drag	0.16	0.33
Pseudo Shear Current	0.30	0.52
Eliminate Truss Drag	0.34	0.59
Towing Tests	0.08	0.19

Table 1 – A/D Values for Sensitivity Cases, 150 deg hdg.

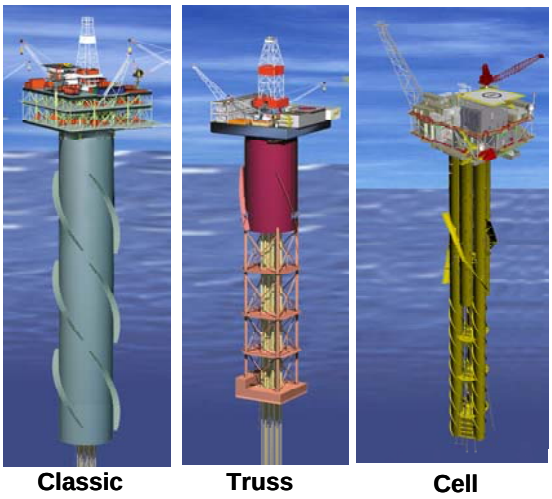

Figure 1 – Types of Spars

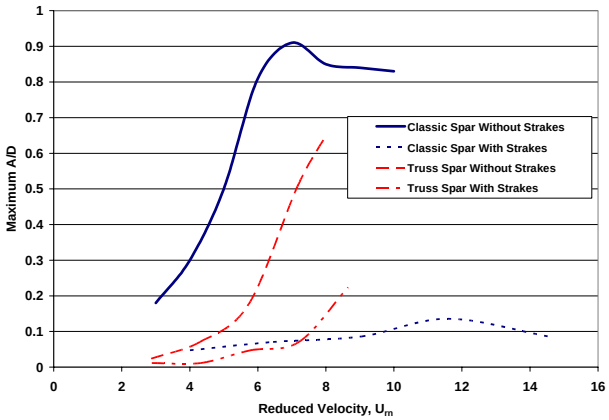

Figure 2 – Typical Spar VIM Response with and without helical strakes

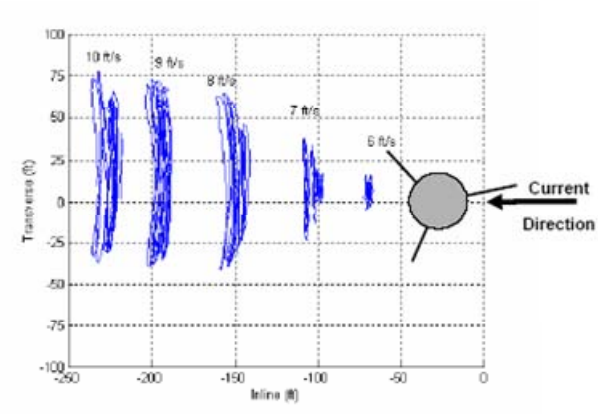

Figure 3 –VIM Response [from 9]

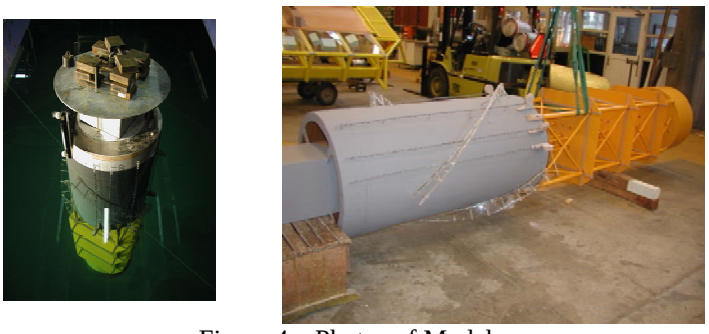

Figure 4 – Photos of Model

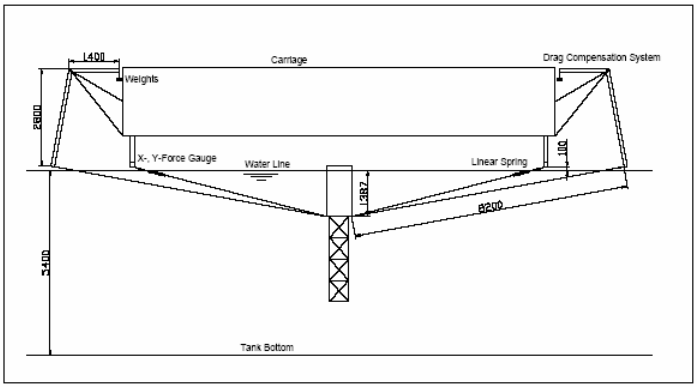

Figure 5 – Side View of Model Towing Arrangement

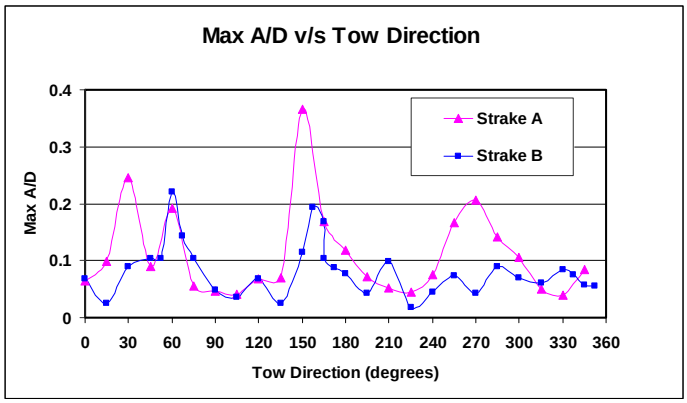

Figure 6 – Comparison of Measured Responses vs. Direction

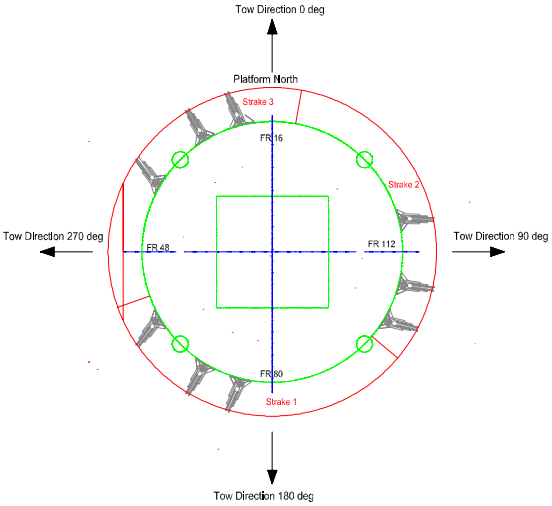

Figure 7 – Towing Directions for Configuration A

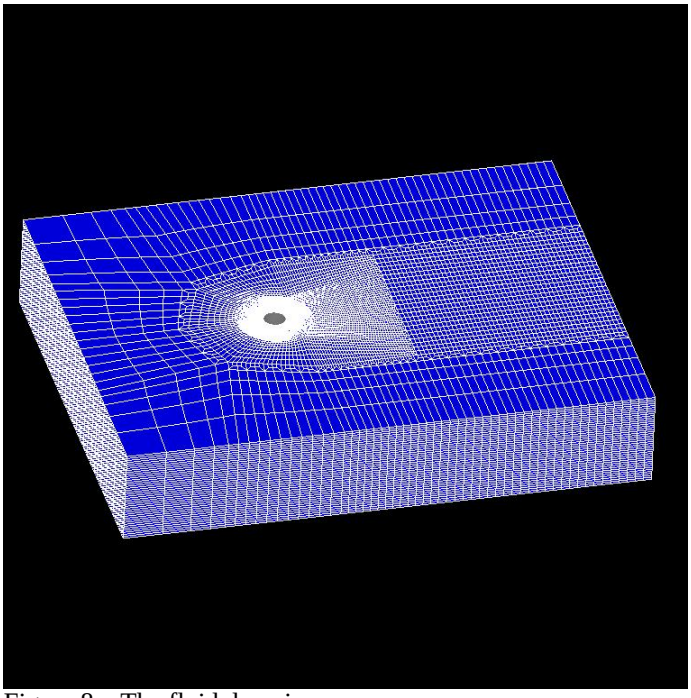

Figure 8 – The fluid domain

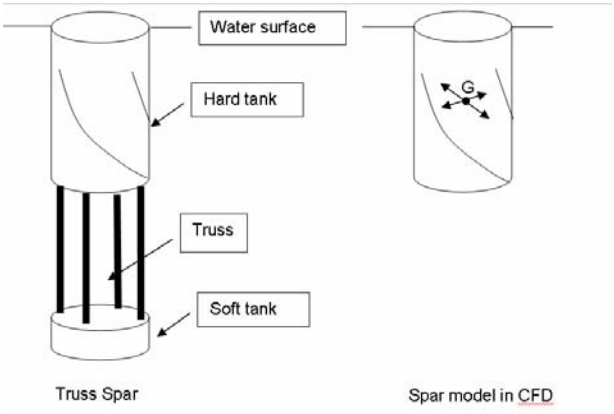

Figure 9 – Hybrid Truss Spar Model

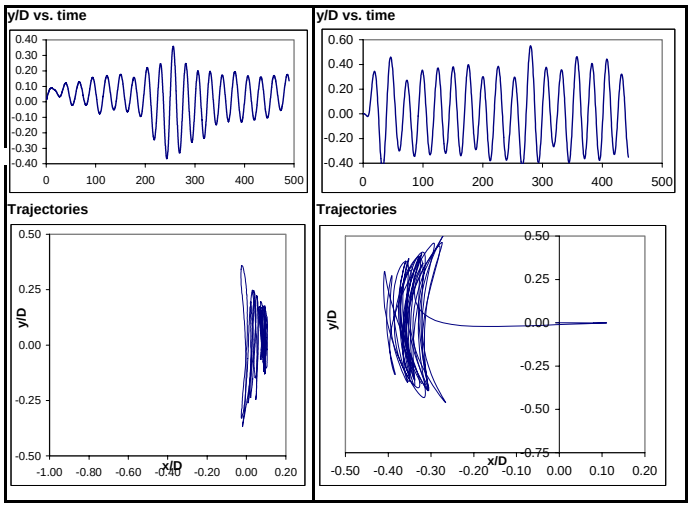

Figure 10 – Comparison of Responses for Peak Response Hdg. = 150 deg, U_{rn} = 8

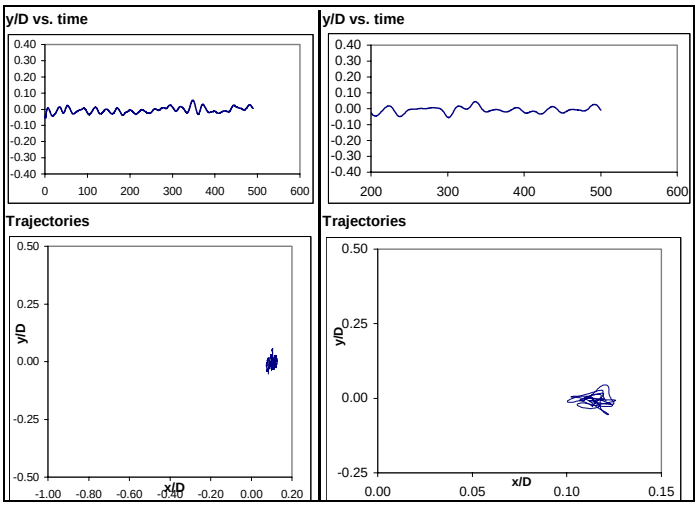

Experiment CFD

Figure 11 – Comparison of Responses for Null Response, Hdg = 330 deg, U_{rn} = 7

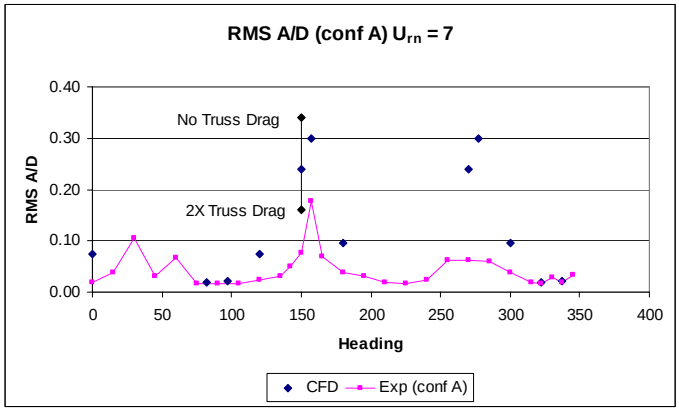

Figure 12 – Configuration A Directional Results

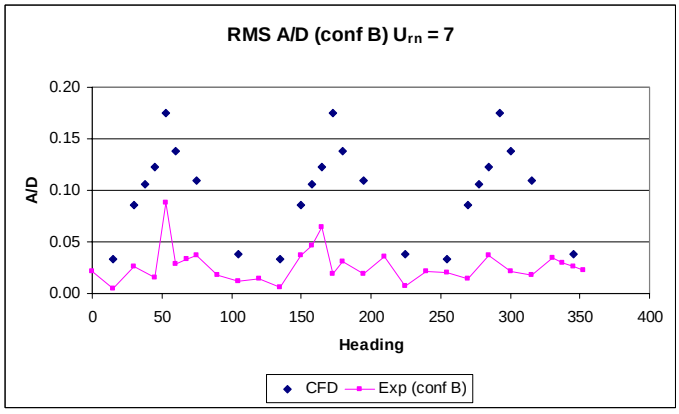

Figure 13 – Configuration B Directional Results

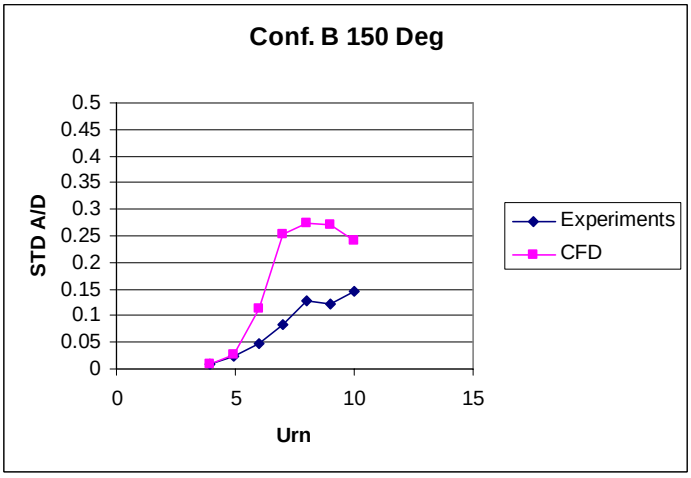

Figure 14 – A/D vs. U_{rn} for Configuration A, 150 deg Hdg.

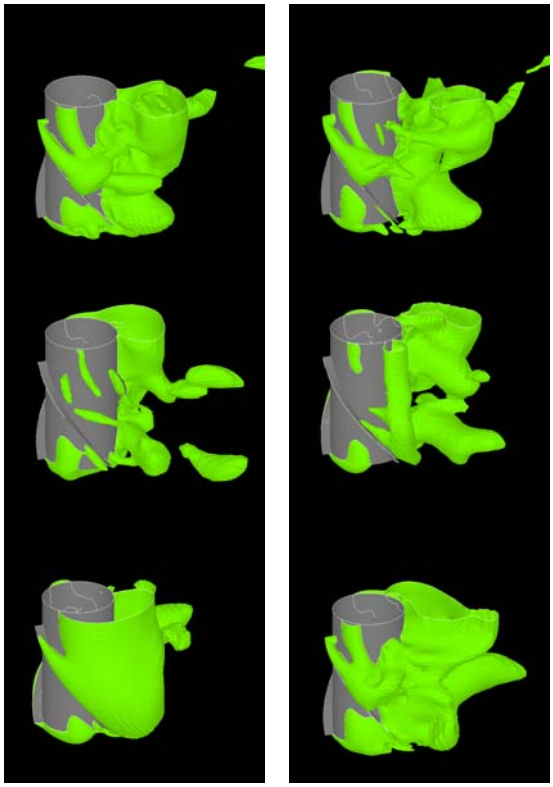

Figure 15 – Flow Visualization for 150 Deg, Configuration A, $U_{rn} = 7$

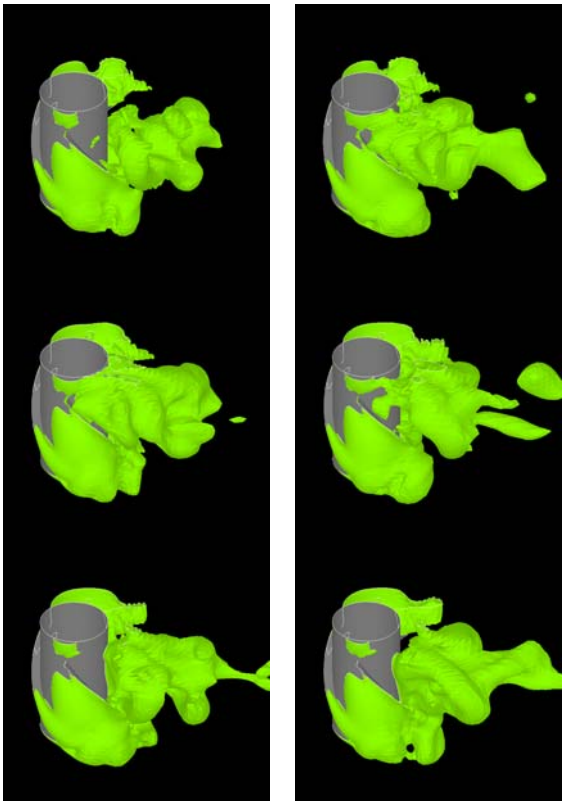

Figure 16 – Flow Visualization for 330 Deg, Configuration A, $U_{rn} = 8$